IMECE2020-23928

ACOUSTIC METAMATERIAL WITH AIR-BACKED DIAPHRAGM FOR BROADBAND ABSORPTION: A PRELIMINARY STUDY

Qian Dong, Xiaolei Song, Subhrodeep Ray, and Haijun Liu¹
Department of Mechanical Engineering, Temple University
Philadelphia, PA, USA

ABSTRACT

Membrane-based acoustic metamaterials have been reported to achieve 100% absorption, the acoustic analogue of photonic black-hole. However, the bandwidth is usually very narrow around some local resonance frequency, which limits its practical use. To address this limitation and achieve a broadband absorption, this paper first establishes a theoretical framework for unit cells of air-backed diaphragms, modeled as an equivalent mass-spring-dashpot system. Based on the impedance match principle, three different approaches are numerically investigated by tuning the cavity length, the static pressure in the cavity, and the effective damping of perforated plates. A prototype with polyimide diaphragm and 3D printed substrate is then fabricated and characterized using an acoustic impedance tube. Preliminary experiments show the feasibility to achieve an absorption bandwidth of ~200 Hz at center frequency of 1.45 kHz. This work pays the way for developing a sub-wavelength light weight broadband acoustic absorber for a variety of applications in noise control.

Keywords: acoustic absorption, metamaterial, metasurface, impedance matching

1. INTRODUCTION

Metamaterials are frequently defined as artificial materials engineered to realize properties that have not been found in nature [1]. Consisting of repeating patterns (a.k.a. unit cells) at scales much smaller than the wavelength of interest, metamaterials provide a new way to manipulate waves through controlling the configuration (size, shape, orientations, etc.) of the unit cells. Similar to its optical counterpart [2,3], acoustic

Among the various types of AMM, a number of membrane-based AMM have been reported to take advantage of its light weight, simple geometry, and the ability to tune the effective density [7]. A typical configuration of the unit cell consists of a clamped membrane (or plate) with or without a mass attached to the center. At the resonant frequencies, the membrane has large displacement/velocity in response to acoustic excitation, which is associated with high transmission. At the anti-resonance frequencies, the membrane has minimum displacement/velocity, acting effectively as rigid reflectors. In terms of the effective density, it is negative below the first resonance frequency.

Applied to acoustic absorption, membrane-based AMM have been demonstrated to obtain almost 100% acoustic absorption at low frequencies [8,9]. For sound in the audible frequency range of 20 Hz to 20 kHz, the viscous dissipation in the vicinity of solid surface, such as plastic foam, glass fiber, and mineral wool, is the conventional method to dissipate the acoustic energy. Since the dissipative force varies linearly as a function of the flux rate, dissipated power (the product of force and flux) is a quadratic function of frequency [10]. Hence, there is a fundamental limitation to achieve high acoustic absorption for low frequency. To this end, AMM provides an alternative approach based on local resonances, where sub-wavelength unit cells can be designed to have resonance frequency in low frequency and be configured to form a large thin panel,

Contact author, narjun@temple.ed

metamaterials (AMM) are designed to manipulate sound waves by tailoring its effective mass density and bulk modulus of the unit cells [4,5]. In recent years, the concept of AMM has been extended beyond the scope of negative refraction materials and found in applications such as acoustic super-resolution, acoustic cloaking based on transformation acoustics, zero-index medium, acoustic meta-surface, and nonreciprocal acoustic devices [6].

¹ Contact author: haijun@temple.edu

potentially addressing the fundamental limit of sound attenuation and absorption.

In a representative example, Sheng and his group demonstrated a membrane based AMM based on hybrid resonances [9]. The unit cell consists of a diaphragm decorated by a rigid center mass and clamped to rigid substrate, a backing gas cavity filled with SF₆, and a rigid aluminum back plate. The presence of the backing gas changes the vibration modes of the membrane (i.e., hybridization). When the membrane tension and depth of the sealed gas cavity are tuned properly, the impedance of the membrane is perfectly matched with air, thus absorbing all the incident energy. Perfect absorption was demonstrated simultaneously at three different frequencies (255, 309, and 420Hz) with three unit cells, each having different center masses (0.18 g, 0.12 g, and 0.06 g) and different gas cavity depths (30 mm, 25 mm, and 15 mm).

However, the absorption bandwidth in most reported AMM is very narrow around some local resonance frequency (e.g. < ~5 Hz in [9]), which limits its practical use. This paper seeks to achieve a fundamental understanding of broadband acoustic absorption using AMM and presents some preliminary numerical and experimental results. In the rest of the paper, we will first establish a theoretical framework for unit cells of airbacked diaphragms based on the impedance matching principle. Here, the term of diaphragm is used as it encompasses pure membrane, pure plate, or cases in between [11]. The goal is to understand the conditions for achieving large absorption bandwidth. Then, three different approaches will be numerically studied, followed by preliminary experimental results.

2. THEORETIAL FRAMEWORK USING IMPEDANCE MATCHING

The focus of this paper is on AMM thin panels with periodic arrangement of unit cells (FIGURE 1(a)) to achieve broadband and high acoustic absorption. As shown in FIGURE 1(b)-(c) for the unit cell, the main component is a circular diaphragm (diameter d and thickness h_d) clamped to a rigid frame and backed by a cylindrical air cavity (length h_c). Based on our previous study on the acoustic-structural interaction [12,13], the combined air-diaphragm system can be modeled as an equivalent mass-spring-dashpot $(m'-s'-R_m')$ system, as illustrated in FIGURE 1(d). The corresponding mechanical impedance is $z'_m = R'_m + j(m'\omega - s'/\omega)$. Assuming the incident plane wave is $p_{in} = P_{in} \exp(j\omega t)$ and the reflected wave is $p_r = P_r \exp(j\omega t)$, the reflection coefficient can be obtained as

$$R = \frac{P_r}{P_{in}} = \frac{Z_m - Z_a}{Z_m + Z_a} = \frac{R_m - \rho_0 c_0 + j(m\omega - s/\omega)}{R_m + \rho_0 c_0 + j(m\omega - s/\omega)},$$
 (1)

where $z_m = z_m'/A = R_m + j(m\omega - s/\omega)$, $z_a = \rho_0 c_0$, A is the effective area of the mass, ρ_0 and c_0 are the density and speed of sound of air, respectively. Therefore, the acoustic absorption can be obtained as follows:

$$\alpha = 1 - |R|^2. \tag{2}$$

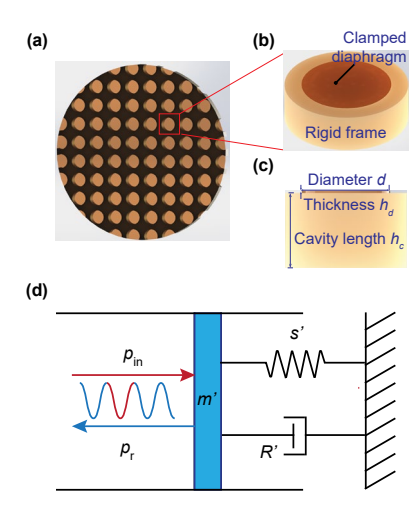


FIGURE 1: Acoustic metamaterial thin panel for broadband acoustic absorption. Schematic of the panel (a) and unit cell (b), whose dimensions are shown in (c) and lumped model in (d).

In order to achieve 100% absorption (i.e., 0% reflection), it can be seen from Eq. (1) that two conditions need to be satisfied (both the real and imaginary parts of the numerator need to vanish): $R_m = \rho_0 c_0$ and $m\omega - s/\omega = 0$, i.e., the impedance of the lumped system matches with that of the air at its resonant frequency $\omega_n = \sqrt{s/m}$. Defining the impedance matching factor as $\beta = R_m/(\rho_0 c_0)$, we can obtain the absorption spectra for different values of β , as shown in FIGURE 2(a) using the parameters listed in Table 1 for a fixed resonant frequency $\omega_n = 1$ kHz. It can be clearly seen that 100% absorption is only achievable when $\beta = 1$, which can also been verified from FIGURE 2(b) where the peak absorption is plot as a function of β using the analytical formula $\alpha_{peak} = 4\beta/(\beta+1)^2$.

In terms of the bandwidth (full width at half maximum), it can be derived as $\Delta\omega=(\beta+1)\rho_0c_0/m$. As seen in FIGURE 2(a), the bandwidth increases when the effective damping increases. More importantly, the bandwidth is inversely proportional to the effective mass. Defining the mass factor η as the ratio of the equivalent mass relative to the nominal value given in Table 1, the absorption spectra for different values of η are studied while keeping the resonant frequency at 1 kHz. It can clearly be seen from FIGURE 2(c)-(d) that increasing the effective mass will lead to smaller bandwidth.

From these results based on the simple lumped model, we can see that the key to obtain a broad absorption bandwidth around a local resonant frequency is to have lighter diaphragm, which is different from most reported membrane-based AMM, typically with a relatively heavy center mass. Based on these insights, we will investigate the use of a single uniform diaphragm to ensure large absorption bandwidth. The focus will then be on how to satisfy the impedance matching condition – tuning the effective damping R_m .

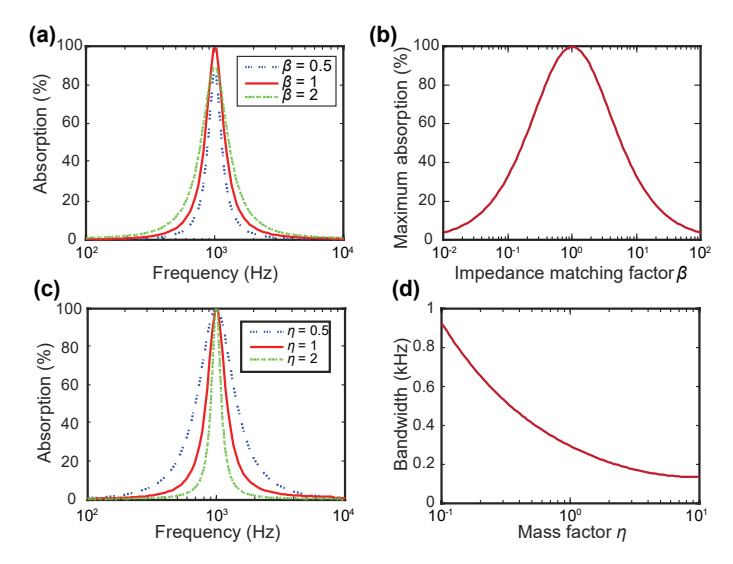


FIGURE 2: Absorption properties of AMM obtained from the analytical lumped model. (a) Absorption spectra for three different values of impedance matching factor β (β = 1 for the matched impedance case). (b) Maximum absorption as a function of β . (c) Absorption spectra for three different values of mass factor η when β = 1 (the bigger the value of η , the heavier the effective mass). (d) Absorption bandwidth as a function of η .

Table 1: Parameters for the analytical lumped model

Density of air $(\boldsymbol{\rho})$	1.24 kg/m^3
Sound speed (c_0)	343 m/s
Cross-section area (A)	707 mm^2
Effective mass (m')	0.25 g
Effective spring constant (s')	9,923 N/m
Resonance frequency (ω_n)	1000 Hz

3. AMM DESIGN USING NUMERICAL SIMULATION

Based on the analysis in Section 2, the effective damping coefficient R_m' needs to be equal to $\rho_0 c_0 A$ so that the real part of the diaphragm's impedance matches with that of air. The question is how to tune the damping given that the intrinsic damping of diaphragm is typically small and constant. We previously studied the acoustic-structural interaction between the diaphragm and the backing cavity, and found that the backing cavity changes the effective mass, stiffness, and damping of the diaphragm [12,13]. In this Section, we will investigate three approaches to tune the effective damping, including the length of backing air cavity h_c , the static pressure of the air cavity p_0 , and the thickness of the perforated plate h_p .

To take into account the viscous loss in the air cavity, a finite element method (FEM) model is developed using the Thermoviscous Acoustic (TA) module in COMSOL 5.3a, which is based on the linearized Navier-Stokes equations. Taking advantage of the symmetry, as shown in the FEM model in FIGURE 3(a), only a 30° segment is modeled: the air cavity is

meshed using second-order brick elements, the diaphragm is meshed using quadrilateral shell elements, and boundary layer meshes are added near all the rigid walls. The diaphragm is made of polyimide film (DuPont Kapton) with a thickness of 1 mil (i.e., 25.4 µm) and diameter of 16.6 mm. A constant Rayleigh damping coefficient $\alpha_0 = 500 \, 1/s$ is used based on our previous experimental results [13]. To excite the diaphragm, a dynamic pressure loading with unit amplitude ($p = e^{i\omega t}$ Pa) is uniformly applied to the outer surface of the diaphragm. The mechanical impedance is calculated by $z_m = p/v$, where v is the average surface velocity of the diaphragm. Thus, the impedance matching factor can be obtained as $\beta = Re(z_m)/$ $(\rho_0 c_0)$. As for controlling the in-plane tension, the diaphragm will be heated in an oven to a higher temperature T while it is glued to a stainless washer. When it is taken out of the oven and cools down to the room temperature T_0 , a uniform tension is generated that is linearly proportional to the shrinkage temperature $\Delta T = T - T_0$. FIGURE 3(b) shows the effect of the backing air cavity in changing the mode shape, i.e., hybridization.

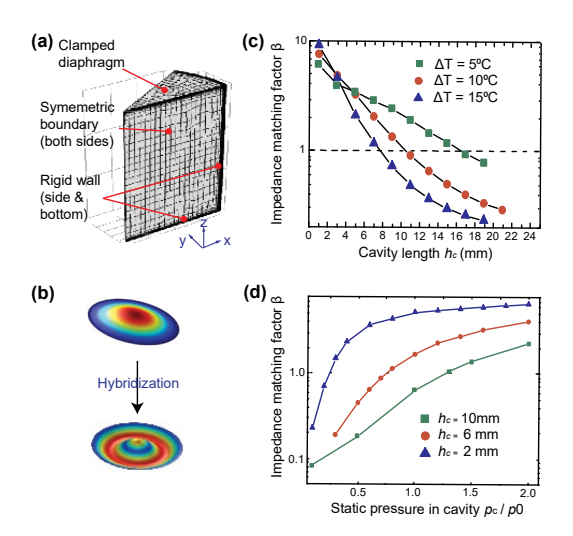


FIGURE 3: Tuning the effective damping using a straight cylindrical air cavity. (a) FEM model in COMSOL. (b) Mode shape of the fundamental mode before (top) and after (bottom) hybridization. (c) Impedance matching factor β as a function of cavity length h_c for three difference shrikage temperatures ΔT . (d) β as a function of the static pressure in the cavity for three different h_c values.

In the first approach, the cavity length h_c will be tuned. FIGURE 3(c) shows the impedance matching factor β as a function of h_c for three different values of ΔT (5°C, 10°C, and 15°C). It can be observed that β increases as the cavity becomes shorter. This can be explained by the value of h_c relative to the boundary layer thickness h_b (69.3 µm thick at 1 kHz). As h_c shrinks and starts to be comparable to h_b , the viscous effects become more pronounced. For diaphragm with larger in-plane tension (larger ΔT such as 15°C), the diaphragm is stiffer and therefore requires a shorter h_c to reach the impedance matching condition ($\beta = 1$). For example the critical value of h_c to ensure $\beta = 1$ is ~8 mm for $\Delta T = 15$ °C, but 17 mm for $\Delta T = 15$ °C, but 17 mm for $\Delta T = 15$ °C, but 17 mm for $\Delta T = 15$ °C.

5°C. Note when the cavity is in the short region ($h_c < \sim 4 \, mm$), the stiffness contributed by the air cavity dominates that of the diaphragm itself. As such the effective damping coefficient is less sensitive to the in-plane tension. That is why the three curves in FIGURE 3(b) almost overlap on each other in this short region.

In the second approach, the static pressure in the backing air cavity p_b is another parameter that can be theoretically used to tune the damping. FIGURE 3(c) shows the impedance matching factor as a function of p_b normalized by the ambient pressure p_0 for three values of h_c (10 mm, 6 mm, and 2 mm) and same ΔT (10°C). In all three cases, as the air particles becomes denser (larger value of p_b), the viscous effect increases, which leads to larger effective damping for the diaphragm.

Different from the above two methods, a third approach adds a perforated back plate in the air cavity, serving similar functionalities in condenser microphones for tuning the effective damping. As shown in the inset of FIGURE 4, a perforated plate with an array of small holes (1 mm for the diameter and 2 mm for the spacing) is added in the middle of the air cavity. Again, TA module in COMSOL is used to simulate the thermoviscous loss at the boundary of small holes. FIGURE 4 plots the impedance matching factor β as a function of the thickness of the perforated plate h_p . The simulation results show that the effective damping increases as the perforated plate becomes thicker.

Among the studied three approaches, the first approach is the simplest and most practical. As such, a preliminary experimental study is conducted to verify the feasibility.

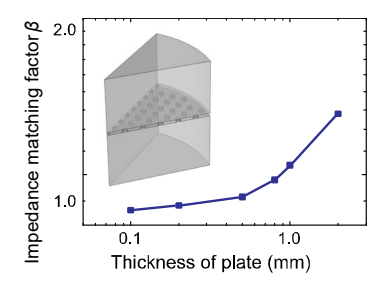


FIGURE 4: Tuning the effective damping by adding a perforated back plate and changing its thickness. Inset shows the schematic in COMSOL.

4. PRELIMINARY EXPERIMENTAL RESULTS

The experimental measurement is based on an impedance tube (Brüel & Kjær 4206-T), as shown in FIGURE 5(a). It features a loudspeaker at one end and four microphones positioned on the side wall (two upstream and two downstream). The test sample is fixed in the middle and an anechoic termination is used to seal the tube end. Instead of using broadband white noise excitation, the approach described in ref. [14] is implemented to use swept sine to ensure better signal-tonoise ratio and more accurate measurements.

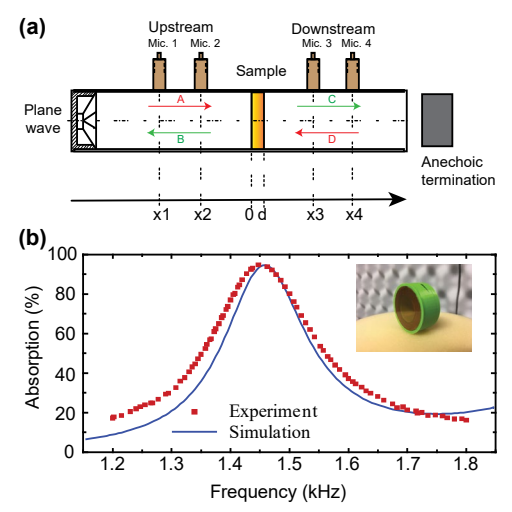


FIGURE 5: Preliminary experimental results. (a) Experimental setup based on an impedance tube (B&K Type 4206). (b) Absorption spectrum for a prototype with 17 mm length cavity.

Based on the simulation results to ensure matched impedance, the cavity length is determined to be 17 mm for shrinkage temperature of $\Delta T = 5^{\circ}$ C. To fabricate the unit cell prototype, first the substrate is 3D printed using polyacrylic (PLA) filaments. Then, a circular 1-mil polyimide film is heated to 5°C above the room temperature in an oven while being glued to a steel shim. When it cools down to the room temperature, a uniform initial tension in generated in the film. Lastly, the steel shim is pressed into a groove in the 3D printed substrate. The back end of the plastic substrate can be considered rigid. See the inset of FIGURE 5(b) for a photo of the prototype.

The measured absorption spectrum is plot in FIGURE 5(b). The peak absorption is found to be 98% at the resonance frequency of 1.45 kHz. More importantly, the bandwidth (FWHM) is found to be 200 Hz, significantly larger than that of AMM with heavy center mass, verifying the feasibility of our approach. The corresponding qualify factor can be calculated as $Q = \sim 7$. To further increase the bandwidth, multiple unit cells can be combined in a single AMM panel, as long as the spacing is much smaller than the wavelength of interest.

5. CONCLUSION

Aiming to address the narrow bandwidth limitation in membrane-based AMM for acoustic absorption, in this paper, we first present a theoretical framework based on the impedance matching principle and describing the diaphragm-and-cavity combination by an effective mass-spring-dashpot model. Through this model, we find that the key to realize large bandwidth is using lighter diaphragm while maintaining the impedance matching condition. We then study three different approaches for tuning the effective damping of unit cells consisting of light and uniform diaphragm backed by an air cavity, including tuning the cavity length, static pressure, and the thickness of an added perforated plate. A preliminary experimental measurement is carried out based on the first

approach and verifies that i) the effective damping coefficient of the diaphragm can indeed be tuned by changing the cavity length to ensure impedance matching, ii) using lighter diaphragm can significantly increase the absorption bandwidth. Further efforts will be devoted to combine various unit cells to have even larger absorption bandwidth so that the developed AMM thin panel can be put into practical applications in noise control and mitigation. Prototypes of the other two approaches will be fabricated in the future to verify the numerical simulations presented in this paper.

6. ACKNOWLEDGEMENTS

This work was supported by the National Science Foundation (grant number: CMMI-1663135).

REFERENCES

- [1] Kshetrimayum, R. S., 2005, "A Brief Intro to Metamaterials," IEEE Potentials, 23(5), pp. 44–46.
- [2] Shelby, R. A., Smith, D. R., and Schultz, S., 2001, "Experimental Verification of a Negative Index of Refraction," Science, **292**(5514), pp. 77–79.
- [3] Smith, D. R., and Kroll, N., 2000, "Negative Refractive Index in Left-Handed Materials," Physical Review Letters, **85**(14), pp. 2933–2936.
- [4] Yao, S., Zhou, X., and Hu, G., 2010, "Investigation of the Negative-Mass Behaviors Occurring below a Cut-off Frequency," New Journal of Physics, **12**(10), p. 103025.
- [5] Li, J., and Chan, C. T., 2004, "Double-Negative Acoustic Metamaterial," Physical Review E, **70**(5), p. 055602.
- [6] Ma, F., Wu, J. H., Huang, M., Zhang, W., and Zhang, S., 2015, "A Purely Flexible Lightweight Membrane-Type Acoustic Metamaterial," Journal of Physics D: Applied Physics, **48**(17), p. 175105.
- [7] Huang, T.-Y., Shen, C., and Jing, Y., 2016, "Membrane-and Plate-Type Acoustic Metamaterials," The Journal of the Acoustical Society of America, 139(6), pp. 3240–3250.
- [8] Mei, J., Ma, G., Yang, M., Yang, Z., Wen, W., and Sheng, P., 2012, "Dark Acoustic Metamaterials as Super Absorbers for Low-Frequency Sound," Nature Communications, 3, p. 756.
- [9] Ma, G., Yang, M., Xiao, S., Yang, Z., and Sheng, P., 2014, "Acoustic Metasurface with Hybrid Resonances.," Nature materials, **13**(9), pp. 873–8.
- [10] Szabo, T. L., 1994, "Time Domain Wave Equations for Lossy Media Obeying a Frequency Power Law," Journal of the Acoustical Society of America, **96**(1), pp. 491–500.
- [11] Yu, M., and Balachandran, B., 2005, "Sensor Diaphragm Under Initial Tension: Linear Analysis," Experimental Mechanics, **45**(2), pp. 123–129.
- [12] Liu, H., Olson, D. A., and Yu, M., 2014, "Modeling of an Air-Backed Diaphragm in Dynamic Pressure Sensors: Effects of the Air Cavity," Journal of Sound and

- Vibration, **333**(25), pp. 7051–7075.
- [13] Dong, Q., Song, X., and Liu, H., 2020, "Effects of Air Cavity in Dynamic Pressure Sensors: Experimental Validation," Sensors, **20**(6), p. 1759.
- [14] Ho, K. M., Yang, Z., Zhang, X. X., and Sheng, P., 2005, "Measurements of Sound Transmission through Panels of Locally Resonant Materials between Impedance Tubes," Applied Acoustics, **66**(7), pp. 751–765.